THE JOURNAL OF BIOLOGICAL CHEMISTRY VOL. 284, NO. 39, pp. 26526–26532, September 25, 2009

ATP Binding to the C Terminus of the *Arabidopsis thaliana* Nitrate/Proton Antiporter, AtCLCa, Regulates Nitrate Transport into Plant Vacuoles*[S]

Received for publication, April 8, 2009, and in revised form, July 27, 2009 Published, JBC Papers in Press, July 27, 2009, DOI 10.1074/jbc.M109.005132

Alexis De Angeli[‡1], Oscar Moran[‡], Stefanie Wege[§], Sophie Filleur[§¶], Geneviève Ephritikhine[§¶], Sébastien Thomine[§], Hélène Barbier-Brygoo[§], and Franco Gambale[‡]

From the [‡]Istituto di Biofisica, Consiglio Nazionale delle Ricerche, Via De Marini 6, 16149 Genova, Italy, [§]Institut des Sciences du Végétal, CNRS, 1 Avenue de la Terrasse, 91198 Gif-Sur-Yvette Cedex, France, and [¶]Université Paris 7-Denis Diderot, UFR Sciences du Vivant, 35 rue Hélène Brion, 75205 Paris Cedex 13, France

Nitrate, one of the major nitrogen sources for plants, is stored in the vacuole. Nitrate accumulation within the vacuole is primarily mediated by the NO_3^-/H^+ exchanger AtCLCa, which belongs to the chloride channel (CLC) family. Crystallography analysis of hCLC5 suggested that the C-terminal domain, composed by two cystathionine β-synthetase motifs in all eukaryotic members of the CLC family is able to interact with ATP. However, interaction of nucleotides with a functional CLC protein has not been unambiguously demonstrated. Here we show that ATP reversibly inhibits AtCLCa by interacting with the C-terminal domain. Applying the patch clamp technique to isolated *Arabidopsis thaliana* vacuoles, we demonstrate that ATP reduces AtCLCa activity with a maximum inhibition of 60%. ATP inhibition of nitrate influx into the vacuole at cytosolic physiological nitrate concentrations suggests that ATP modulation is physiologically relevant. ADP and AMP do not decrease the AtCLCa transport activity; nonetheless, AMP (but not ADP) competes with ATP, preventing inhibition. A molecular model of the C terminus of AtCLCa was built by homology to hCLC5 C terminus. The model predicted the effects of mutations of the ATP binding site on the interaction energy between ATP and AtCLCa that were further confirmed by functional expression of site-directed mutated AtCLCa.

Nitrate is among the major nitrogen sources for plants in aerobic soils. It is taken up by root cells through plasma membrane transporters of nitrate-nitrite transporter and peptide transporter families. Once in the cytoplasm it can enter the amino acid biosynthesis pathway (1) or be accumulated in the vacuolar lumen via tonoplast transporters (2).

The vacuolar nitrate transporter of the model plant *Arabidopsis thaliana*, AtCLCa, has been shown to work as an anion/proton antiporter (3, 4), similarly to the bacterial CLCec-1 (5) and human hCLC-4 (6) as well as hCLC-5 (7). However, whereas bacterial and animal CLCs[2] transport chloride ions, the AtCLCa antiporter is more selective for nitrate, and therefore, it is able to mediate the accumulation of nitrate into the plant vacuole.

Little is known on the modulation of CLC-proteins by nucleotides. The effects of ATP on the ion channel hCLC-1 are a matter of debate (8). Indeed, some reports have shown that ATP inhibits hCLC-1 currents, probably interacting with the C terminus of the protein (9–11). Conversely, other reports indicate that ATP does not modify the properties of hCLC-1 current (12). This discrepancy has been attributed to the oxidation state of the channel, as ATP would be effective only in the presence of reducing agents (13).

The C terminus domain of all eukaryotic CLC proteins has two cystathionine β-synthetase motifs (CBS (14, 15)), each one characterized by a βαββα topology (16, 17). A structural and biochemical study of the hCLC-5 C-terminal part demonstrates that this region binds nucleotides (14). However, the effect of ATP binding on the transport activity of hCLC-5 is still unknown.

The presence of analogous CBS domains in the C terminus of the AtCLCa antiporter suggested the hypothesis that ATP binds to this plant transporter and modulates its transport activity. Hence, we undertook a functional analysis of the effect of adenosine nucleotides on AtCLCa and found that ATP inhibits the AtCLCa-mediated transport. Based on a homology model of the C terminus of the channel, we identified two residues that would be putatively involved in the protein-nucleotide interaction.

EXPERIMENTAL PROCEDURES

Electrophysiology—Protoplasts and vacuoles were extracted from *A. thaliana* leaves as described elsewhere (3). *AtCLCa* cDNA was cloned from Col-0 ecotype into the *pfunct+Tag* vector (18) (supplemental material). Col-0 cDNA was used to have the TAIR sequence for checking cloning efficiency. The *pfunct+Tag* was used to allow the recognition of transformed protoplasts without tagging the protein (supplemental material). For transient transformation of *clca-2* knock-out proto-

* This work was supported by EU_RTN Project VaTEP Contract MRTN-CT-2006 035833 and Consiglio Nazionale delle Ricerche-CNRS bilateral project "Biophysical properties of the AtCLCa antiporter in *A. thaliana*."

[S] The on-line version of this article (available at http://www.jbc.org) contains supplemental Figs. 1–4, Table 1, and additional material.

[1] Present address: Institute for Plant Biology, University of Zürich, CH-8008 Zürich, Switzerland. To whom correspondence should be addressed. Tel.: 41446348286; Fax: 41446348204; E-mail: deangeli@access.uzh.ch.

[2] The abbreviations used are: CLC, chloride channel; CBS, cystathionine β-synthetase; Bis-Tris, 2-[bis(2-hydroxyethyl)amino]-2-(hydroxymethyl)propane-1,3-diol; MES, 4-morpholineethanesulfonic acid; BafA1, bafilomycin A_1; ATPγS, adenosine 5′-*O*-(thiotriphosphate); pF, picofarads.

plasts we followed the specific transformation protocol described in De Angeli *et al.* (19). Transformed protoplasts were individually selected by fluorescence detection, and the corresponding vacuole was isolated under the microscope.

Patch clamp experiments were made in the whole-vacuole configuration with an access resistance between 1.5 and 3 megaohms. Patch clamp recordings were made with an Axon 200A amplifier (Axon Instruments, Sunnyvale, CA). Data were acquired with an AD/DA converter Instrutech ITC16 under the control of the software Pulse (HEKA, Lambrecht-Pfalz, Germany) and analyzed with in-house programs developed under the Igor Pro environment (Wavemetrics, Lake Oswego, OR).

Currents were evoked by 5-s pulses from −77 to +43 or +83 mV in +20-mV increments followed by a 3-s tail pulse to +33 mV. Holding potential was kept at −17 mV. Potential was always corrected by the liquid junction potential (20). Current-to-voltage characteristics were obtained measuring the amplitude of the stationary current. When solutions were changed, measurements were done after 15 min of perfusion. Bis-Tris-propane was chosen as a large impermeable cation to minimize cation currents. Currents were normalized to the current measured at +43 or at +63 mV in reference solutions and expressed as current density per membrane capacitance.

The solution used for patch clamp experiments were as follows. 1 standard vacuolar solution: 100 mM Bis-Tris-propane, 200 mM HNO_3, 1 mM $CaCl_2$, 5 mM $MgCl_2$, 5 mM MES, pH 5.5; 2-standard cytosolic solutions: control 7.5 mM Bis-Tris-propane, 15 mM HCl, 0.1 mM $CaCl_2$, 2 mM $MgCl_2$, 15 mM MES, pH 7, with 100 nM bafilomycin A_1 (BafA1) as indicated; 3-nitrate solution: 0.1 mM $Ca(NO_3)_2$, 2 mM $Mg(NO_3)_2$, 15 mM MES, pH 7 with Bis-Tris-propane, BafA1 as indicated. Osmotic pressures of the cytosolic and vacuolar solutions were adjusted with sorbitol to 640 and 590 mosM, respectively. Nucleotides (Sigma) were added to the bath cytosolic solution in the salt form as Mg-ATP, Na_2-ATP, Tris-ATP, Na_2-ADP, Na-AMP, Li_4-ATPγS. After the addition of nucleotides the pH of the solution was adjusted with Bis-Tris-propane to reach the correct value. Solutions with nucleotides were daily prepared, maintained at 4 °C, and warmed to room temperature before use. BafA1 was obtained from Wako (Neuss, Germany), dissolved in DMSO in a 140 μM stock solution, stored at −20 °C, and added daily to the patch solutions to a final concentration of 100 nM.

To calculate the apparent dissociation constant (K_d), the Langmuir isotherms were fitted with the equation,

$$I_{norm} = 1 - \frac{I_{inh}}{1 + \frac{K_d}{[ATP]}} \qquad \text{(Eq. 1)}$$

where I_{norm} is the steady state current normalized to the value at +63 mV, and I_{inh} is the maximum fraction of current inhibited by ATP.

Molecular Modeling—Homology modeling was done by fitting the primary sequence of the C terminus of the AtCLCa antiporter (SwissProt P92941) to the structure of the human CLC-5 C terminus (hCLC-5 PDB accession code 2J9L), solved by x-ray crystallography at 3 Å resolution (15). Structural fitting was performed using Swiss-Model server (21). Further refinements, including the search for side-chain rotamers, reconstruction of loops, and preliminary energy minimization, were done using Swiss PDB Viewer (22). The model modifications to introduce single point mutations were done using the Swiss PDB Viewer software. Final energy minimization was performed by NAMD software (23) (see the supplemental material) using the force filed AMBER99.

The free and bound nucleotides (ADP and ATP) were considered in their fully ionized forms: ATP^{4-} and ADP^{3-} (which represent ~60% of the total ATP and ADP at pH 7). Each C terminus model (hCLC-5, AtCLCa) was located in the center of a water sphere of 47 Å radius. For the free nucleotides (ATP, ADP, and AMP) the radius of the simulation sphere was 20 Å. The water in the simulation sphere was defined at a density of 0.998 g/liter. Water molecules in the 4 Å external shell were restrained with an harmonic force of 50 kcal $mol^{-1}Å^2$, and the inner 4 Å shell was restrained with a force of 5 kcal $mol^{-1}Å^2$. The system was neutralized with the addition of Na^+ ions. The system was minimized, gradually heated to 300 K, and successively used for molecular dynamics (supplemental material).

Molecular dynamics trajectories were inspected to assess stability, *i.e.* the average internal energy of the system was required not to change significantly during the simulation (supplemental Fig. 4). The calculation of the free energy of binding (ΔG_{bind}) was done with the linear interaction energy approximation method (24, 25) (supplemental material). ΔG_{bind} was calculated as

$$\Delta G_{binding} = \alpha \Delta V_{l-s}^{(vdW)} + \beta \Delta V_{l-s}^{(elec)} + \gamma \qquad \text{(Eq. 2)}$$

where α and β are weighted parameters of the nonpolar and polar binding energies contributions, respectively, and γ is an additional parameter. $\Delta V_l^{x}{}_{-s}$ stands for the difference of the ensemble averages of electric and van der Waals (vdW) energy between the ligand bound to the protein and free in solution. α, β, and γ parameters have been determined for different sets of proteins and ligands (24–27) (see the supplemental material).

RESULTS

ATP Inhibits AtCLCa Current and Activates Proton Pumps on the Same Vacuole—As previously described (3), currents measured in vacuoles from protoplasts that constitutively express AtCLCa in an ATP-free solution are characterized by an initial relaxation followed by a stationary component, with a current density of 7.5 ± 1 pA/pF measured at +43 mV and a reversal potential of −43 ± 2 mV (n = 15).

In 6 independent experiments we observed that the application of 5 mM Mg-ATP to the cytosolic side of the vacuolar membrane led to an initial 6–25% increase of the steady-state current followed by a decay to a final amplitude of 44 ± 2% (Fig. 1, *a* and *b*). When a similar protocol was applied to experiments conducted on vacuoles extracted from *clca-2* knock-out plants, we observed only an increase of the stationary current to a value of 2.3 ± 0.4 pA/pF (n = 4), as shown Fig. 1*c*. The current increase in *clca-2* knock-out preparation is comparable with that mediated by the H^+-ATPase (28). To test whether the initial current increase recorded on wild type vacuoles could be attributed to a stimulation of H^+-ATPase by ATP, we carried

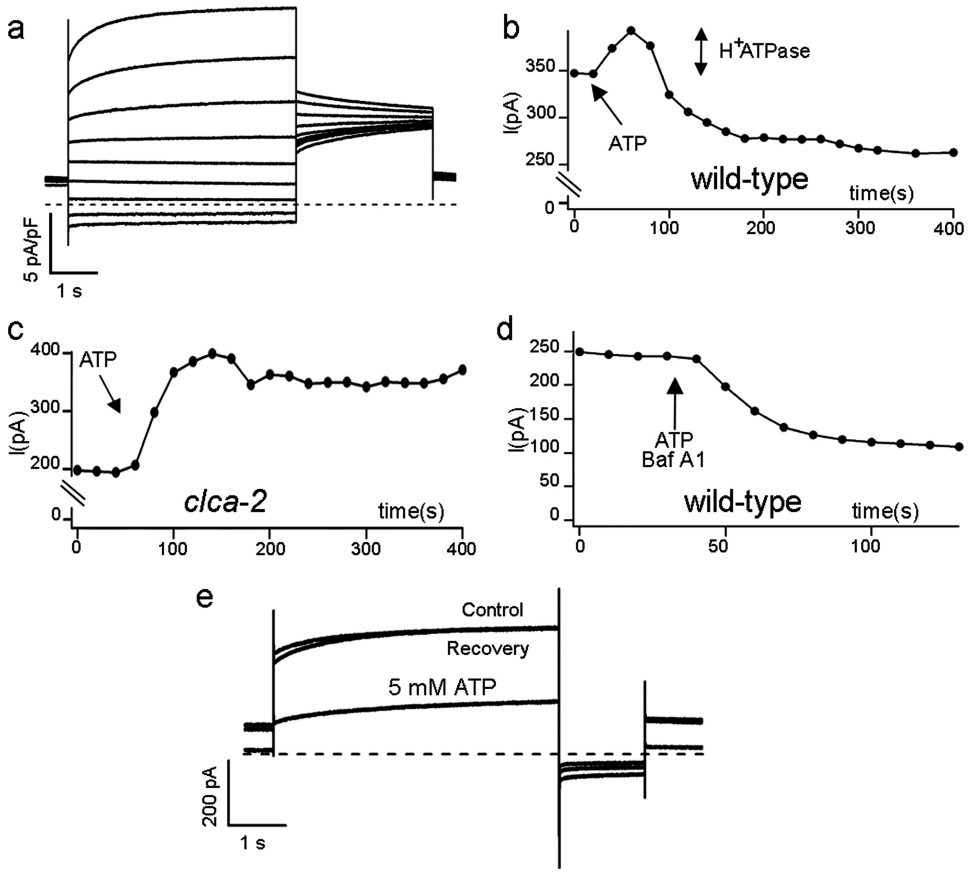

FIGURE 1. **Cytosolic ATP regulates AtCLCa currents in a reversible manner.** *a*, AtCLCa currents recorded in a wild type vacuole in response to 5-s pulses from −77 to +83 mV in +20-mV increments followed by a 3-s tail to +33 mV. *b*, steady state currents measured every 10 s at +43 mV in a wild type vacuole; the *arrow* indicates the addition of ATP. The addition of 5 mM Mg-ATP to a wild type vacuole resulted in an initial transient increase (indicated by the *double arrow*), possibly because of H^+-ATPase activation, followed by a current decay. *c*, the same experiment was conducted on vacuoles from the *clca-2* knock-out mutant, where only the increase of current due H^+-ATPase activation could be observed. *d*, 5 mM Mg-ATP was added to a wild type vacuole in the presence of the H^+-ATPase inhibitor BafA1 (100 nM). *e*, current recordings obtained in control conditions after the addition of 5 mM Mg-ATP at the cytosolic side of the membrane and after recovery by 3 min of perfusion to wash away ATP. Membrane potential stimulation were applied every 10 s as follows; holding at 0 mV, a first pulse at +43 mV for 5 s, and a tail pulse to −33 mV for 1 s. The *dashed line* represents zero current level.

out the same experiment in the presence of the vacuolar H^+-ATPase inhibitor BafA1 (29). As presented in Fig. 1*d*, in the presence of BafA1, the transient increase of the current was absent, thus confirming that this variation of the current was because of the activation of the vacuolar H^+-ATPase. Therefore, to get rid of the activation of H^+-ATPase and to isolate the effect of Mg-ATP on AtCLCa, we added 100 nM BafA1 in all subsequent experiments. Fig. 1*e* shows the reversible reduction of the anion current (in the presence of 100 nM BafA1) after perfusion of isolated vacuoles with 5 mM Mg-ATP.

Nucleotide Effects on the Properties of AtCLCa Current—Fig. 2*a* shows current traces of AtCLCa recorded in the presence of 100 nM BafA1 in control conditions (*left panel*) and after perfusion with 5 mM Mg-ATP (*right panel*). The normalized I/V curves presented in Fig. 2*b* show that ATP inhibits both inward currents (Cl^- influx to vacuole) and outward currents (NO_3^- efflux from the vacuole). Mg-ATP at 5 mM induces a 59 ± 6% inhibition of the total current at +43 mV and a 55 ± 10% inhibition at −77 mV ($n = 6$). The presence of Mg-ATP also modifies the reversal potential of the AtCLCa current from −43 ± 2 mV ($n = 6$) in control conditions to −29 ± 3 mV (Fig. 2*b*). The shift of the reversal potential can be explained by an increase of the relative contribution of nonspecific leakage currents when the number of active transporters is reduced by ATP or by a conformational change induced by ATP that would modify the selectivity of the transporter. We measured the apparent dissociation constant for ATP, K_d, yielding 49 ± 6 μM at +43 mV. Fig. 2*c* shows the fit of data obtained at three different potentials with a Langmuir isotherm. The K_d is almost voltage-independent (Fig. 2*c*, *inset*, the slope of the continuous line is 0.10 ± 0.08 μM/mV), thus indicating that the ATP binding site is possibly located out of the transmembrane electric field. Na-ATP, Tris-ATP, and ATP-γ-S induced an inhibition comparable with that induced by Mg-ATP (supplemental Fig. 1), hence suggesting that the current reduction because of Mg-ATP is independent of Mg^{2+} and probably does not imply ATP hydrolysis.

As the antiporter AtCLCa drives the influx of nitrate into the vacuolar lumen *in vivo* (3), we performed experiments in the presence of NO_3^- at the cytosolic side of the membrane to directly measure the influx of nitrate into the vacuole and verify whether 5 mM Mg-ATP is able to inhibit NO_3^- influx too. Fig. 3 shows the I/V characteristics in control conditions and in the presence of 4.2 mM NO_3^- and 4.2 mM NO_3^- plus 5 mM Mg-ATP in the cytosolic solution. As previously reported (3), cytosolic NO_3^- shifted the reversal potential to −20 mV, increasing the negative component of the current (*i.e.* NO_3^- entering the vacuole). Similarly to what is reported in Fig. 3, the inhibition of the current by 5 mM Mg-ATP was 50 ± 6% ($n = 3$) at −77 mV in NO_3^- and 40 ± 10% at +43 mV ($n = 3$), an effect of the same order of magnitude as ATP inhibition when Cl^- was present at the cytosolic side of the tonoplast.

Application of AMP and ADP to the cytosolic side of the vacuolar membrane did not produce significant effects on AtCLCa currents. Indeed, inhibition of the current measured at +43 mV by 5 mM ADP was 6 ± 2% ($n = 4$) and by 5 mM AMP was 9 ± 2% ($n = 4$). To test for the competition between nucleotides, we added an excess of Na-AMP or Na-ADP (*i.e.* 1 mM) to solutions containing 0.1 mM Mg-ATP. The inhibition of the current induced by 0.1 mM Mg-ATP (39 ± 9% at +43 mV; $n = 4$) was not affected by the addition of 1 mM Na-ADP (35 ± 10%; $n = 3$), whereas inhibition by ATP was almost abolished by 1 mM Na-AMP (9 ± 8%; $n = 3$).

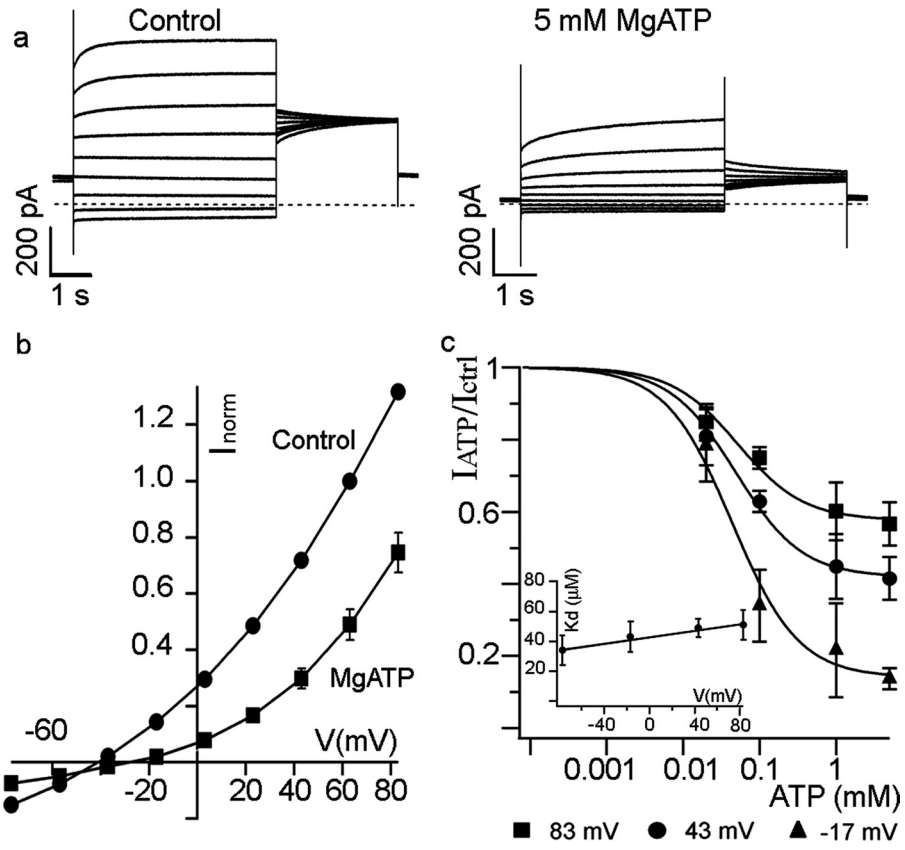

FIGURE 2. **ATP decreases both the inward and outward anion currents.** *a*, anion current families (evoked as in Fig. 1*a*) in control conditions (*left*, see "Experimental Procedures") and in the presence of 5 mM Mg-ATP and 100 nM BafA1 (*right*). The *dashed lines* represent the zero current level. *b*, normalized I-V curves ($n = 6$) in control conditions (●) and in 5 mM Mg-ATP + BafA1 (■). Note that ATP inhibition acts both on Cl^- influx and NO_3^- efflux. *c*, dose response curves for Mg-ATP at different membrane potentials: ■, +83 mV; ●, +43 mV; ▲, −17 mV (data corresponding to −77 mV are not shown for clarity reasons). *Inset*, the apparent dissociation constant (K_d) plotted against the membrane potential is not voltage-dependent. *Bars* correspond to S.E. ($n = 3–6$). Vacuolar and cytosolic standard solutions added with ATP as indicated (see "Experimental Procedures").

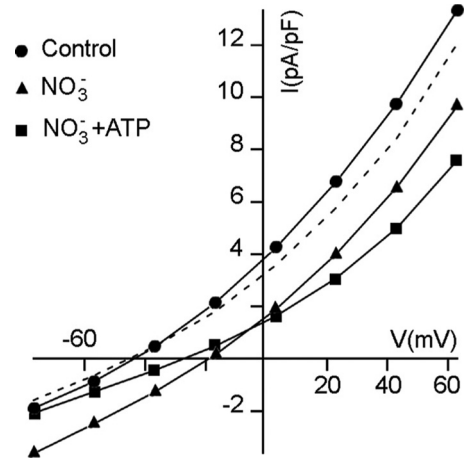

FIGURE 3. **ATP decreases the uptake of nitrate from the cytosol.** I-V relationship of an experiment performed to visualize the NO_3^- influx and its inhibition by Mg-ATP. ●, control (*i.e.* 15 mM HCl); ▲, 4.2 mM NO_3^- at the cytosolic side; ■, 4.2 mM NO_3^- plus 5 mM Mg-ATP, *dashed line* recovery from NO_3^- + ATP to control. Vacuolar and cytosolic standard solutions and nitrate cytosolic solution were added with ATP as indicated (see "Experimental Procedures"). Results are shown for one representative vacuole over three.

Molecular Modeling of the AtCLCa C Terminus—To provide a structural background to the hypothesis that the C terminus of AtCLCa is involved in nucleotide binding, we constructed a homology model of AtCLCa based on the structure of this C-terminal region reported for hCLC-5 (15). Alignment of AtCLCa and hCLC-5 sequences is shown in Fig. 4*a*. The AtCLCa model included an ATP molecule in the same position as the template. Superimposition of the final model and the template backbones yields a root mean square deviation of 1.5 Å. The quality of the geometrical properties of the model was evaluated using PROCHECK (30) and WHATIF (31) packages.

In hCLC-5, the ATP binding site is located at the interface between the two CBS domains (15), with the adenine moiety deeply inserted into the protein and the phosphate groups interacting with some residues of the domain (supplemental Figs. 2 and 3; see also Meyer *et al.* (15)). In this configuration, residues in position 617 and 727 are described to be involved in ATP binding, in agreement with the fact that mutations Y617A and D727A abolish ATP binding to hCLC-5 (15). In the AtCLCa model, the equivalent residues H620 and D753 are also close to ATP (Fig. 4*b*).

Mutations in the C-terminal Domain of AtCLCa Alter ATP Effects on the Nitrate Current—Based on this AtCLCa model, we designed two site-directed mutagenesis experiments in an attempt to perturb the putative ATP binding site in the C terminus of AtCLCa. Mutations H620A and D753A were transiently expressed in *clca-2* knockout protoplasts (19). Mutant protoplasts transfected with wild type AtCLCa were used as a control. Fig. 5*a* shows traces of the current recorded in vacuoles transiently transfected with wild type AtCLCa, showing similar electrophysiological properties as described for endogenous AtCLCa currents. The AtCLCa current presents both the transient and stationary components, a high current density of 63 ± 16 pA/pF at +43 mV, and a reversal potential of −50 ± 5 mV ($n = 3$) (19). The addition of 5 mM MgATP to the cytosolic solution led to an inhibition of 65 ± 9% of the wild type AtCLCa current measured at +43 mV, which is comparable with the inhibition observed for the endogenous antiporter. Vacuoles transfected with D753A displayed currents similar to the wild type (Fig. 5*b*), with a current density of 71 ± 10 pA/pF and a reversal potential of −44 ± 3 mV. In contrast with the strong inhibition by ATP observed in vacuoles expressing the wild type AtCLCa, the addition of 5 mM Mg-ATP to cytosolic solution induced a negligible inhibition of the current of 9 ± 7% ($n = 4$) in vacuoles expressing the D753A mutant of AtCLCa. In the absence of ATP, mutant H620A also showed currents similar to those of wild type-transfected pro-

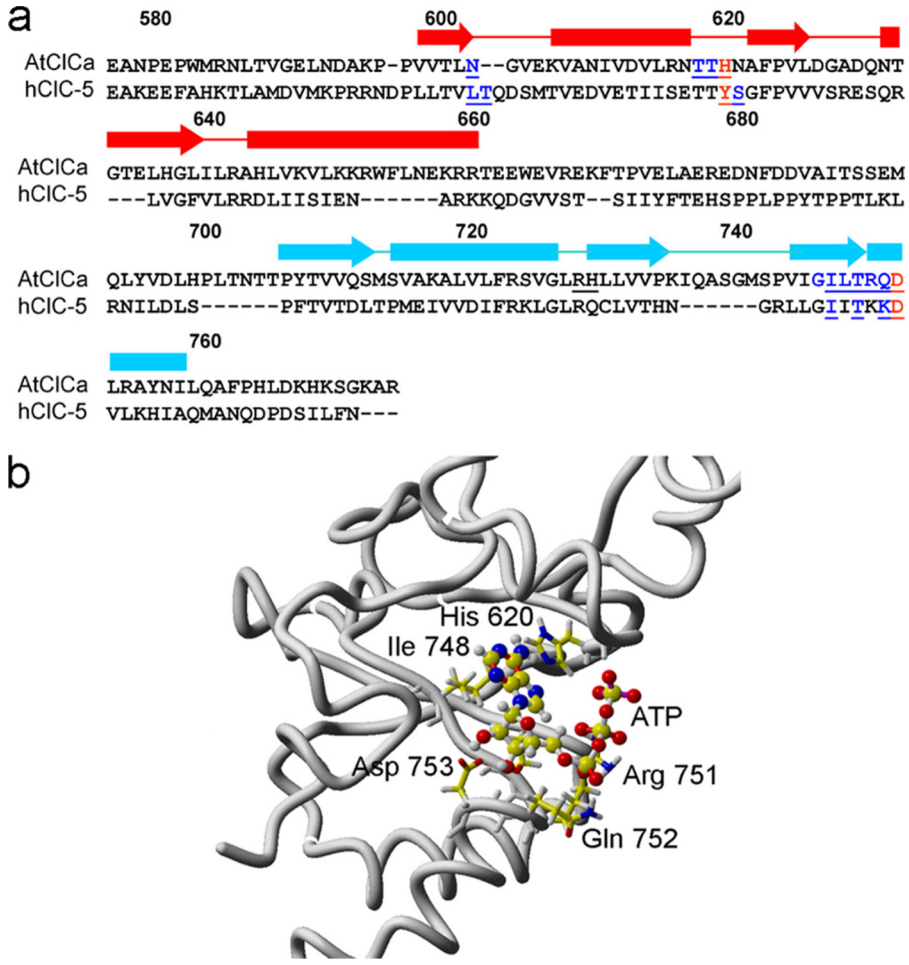

FIGURE 4. **Homology model of the AtCLCa C-terminal region.** *a*, the alignment used for the homology modeling of AtCLCa C-terminal region on the hCLC-5 C-terminal region. Numbering of the amino acid residues corresponds to AtCLCa. *Arrows* and *blocks above the sequences* represent the α-helices and the β-sheets of hCLC-5, respectively (*red*, CBS1; *blue*, CBS2). *Underlined residues* are putatively involved in nucleotide interaction in both proteins. Residues which have been mutated are shown in *red*. *b*, detail of the region putatively involved in the ATP-AtCLCa interaction. His-620 and Asp-753 in AtCLCa correspond to Tyr-617 and Asp-750 in hCLC5 (see *panel a*), which have been shown to be important for nucleotide binding (15).

toplasts (Fig. 5*c*) (current density of 84 ± 20 pA/pF and a reversal potential of −47 ± 1 mV), but the addition of 5 mM MgATP induced a current inhibition of 55 ± 5% (n = 3), which is close to the inhibition obtained in wild type-transformed vacuoles.

Estimation of the Free Energy of Binding in the Molecular Models—To provide a further support to the hypothesis of binding of nucleotides to the C terminus of AtCLCa, we evaluated the free energy of binding ($\Delta G_{binding}$) of ATP in the molecular models using the semi-empirical lineal integration of energy method (24, 25). The energy terms for the calculation were obtained from the time ensemble deduced from a molecular dynamics simulation. We used the parameters $\alpha = 0.476$, $\beta = 0.165$ and $\gamma = 0$, obtained by Jones-Hertzog and Jorgensen (26), as those that better approach with the experimental data obtained for hClC5 ($\Delta G_{binding}$ is about 5.5 for all three nucleotides). Other parameter sets yielded the same qualitative results (see the supplemental material).

We examined the variation of the binding free energy, $\Delta\Delta G_{binding}$, as a representative quantity that expresses the change of the affinity of a given nucleotide to the protein binding site. Although a relatively small change in $\Delta G_{binding}$ of about 4 kcal/mol was seen when comparing the free energy of binding for AMP and ATP in AtClCa, a more pronounced change of −13.8 kcal/mol was observed when comparing $\Delta G_{binding}$ of ADP and ATP (see Table 1). This result is qualitatively consistent with the experiments of ATP displacement, where ADP does not efficiently remove the ATP inhibitory effect, whereas it is almost completely abolished by application of AMP (see above).

Estimation of the binding free energy in the *AtCLCa* model with mutation D753A yielded a severe reduction of the affinity, with a $\Delta\Delta G_{binding}$ of −17.7 kcal/mol, in agreement with the lack of ATP effect in this mutant. Conversely, a more reduced $\Delta\Delta G_{binding}$ of −5.8 kcal/mol was observed comparing the binding free energy of mutant H620A and the wild type models.

DISCUSSION

The interaction between channels or antiporters of the CLC family and ATP is still a matter of debate, and the physiological role of this interaction is not understood yet (8). The binding site for nucleotides in hCLC-5 has been hypothesized to be located at the interface of the two CBS domains in the C-terminal region of the protein (10). A similar CBS motif is present in the C terminus of the plant AtCLCa antiporter (Fig. 4). AtCLCa offers the unique possibility of studying a CLC transporter in its native membrane, the tonoplast, with the advantage that the orientation of the tonoplast exposes the C terminus of AtCLCa to the cytosolic bath solution. This allows us to directly study the cytosolic side of a CLC protein in the whole-vacuole configuration by the patch clamp method.

In this work we found that the AtCLCa current was reversibly inhibited by micromolar concentrations of ATP added at the cytoplasmic side of the vacuolar membrane. Conversely, no current decrease was observed on *clca-2* knock-out mutant vacuoles (Fig. 1), thus suggesting that ATP exerts an inhibitory effect on the transport mediated by the AtCLCa protein. Functional determination of the apparent dissociation constant of ATP from AtCLCa yielded 49 μM, which is on the same order of magnitude of the dissociation constant determined for the CBS domains of CLC-5 (*i.e.* 90 μM), measured by equilibrium dialysis (15). The voltage independence of the K_d for ATP binding to AtCLCa demonstrates that the binding site is located outside

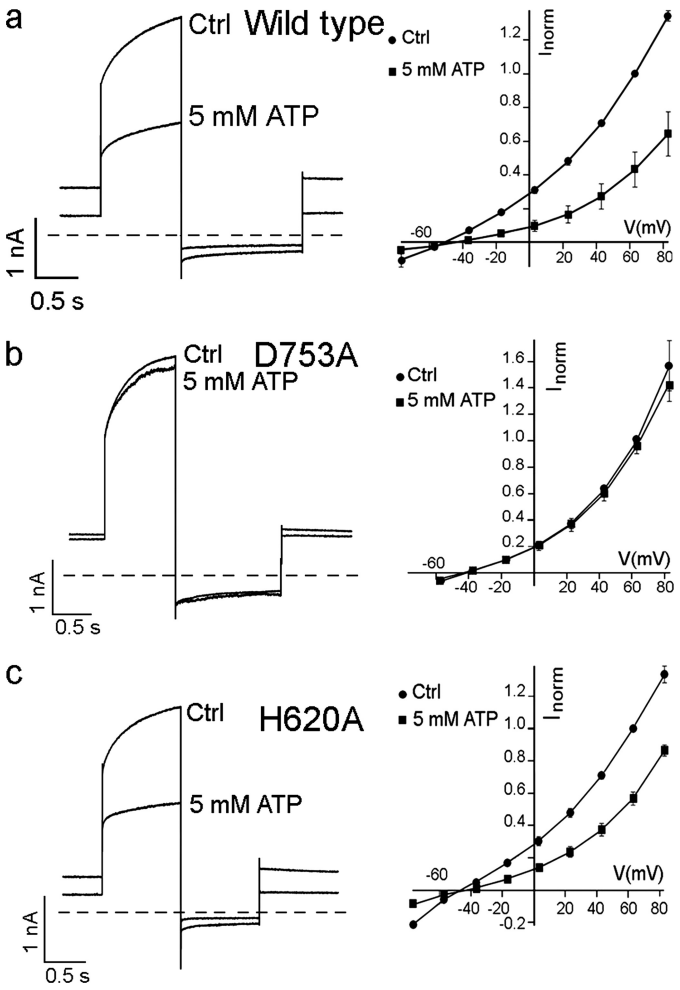

FIGURE 5. **AtCLCa C terminus is involved in the interaction with ATP.** Anion currents (*left panels*) and I/V characteristics (*right panels*) measured in *clca-2* knock-out mutant vacuoles extracted from protoplasts transiently transfected with wild type *AtCLCa* (*a*), *D753A* (*b*), and *H620A* mutants (*c*). *a*, currents recorded in vacuoles transfected with wild type AtCLCa showed an inhibition by 5 mM ATP comparable with that observed in Fig. 2. *b*, vacuoles transfected with the D753A mutants displayed an inhibition of the current by 5 mM ATP that is greatly diminished. *c*, vacuoles transfected with the H620A mutants instead are inhibited by 5 mM ATP in a way comparable with wild type (see *panel a*). Vacuolar and cytosolic standard solutions added with ATP as indicated (see "Experimental Procedures"). For I-V curves, mean I values ± S.E. are shown ($n = 3–4$). *Ctrl*, control.

TABLE 1

Estimates of the van der Waals (ΔV^{vdW}_{l-s}) and electrostatic (ΔV^{elec}_{l-s}) terms of the potential energy differences of bound and free nucleotides, expressed in kcal/mol

Data are the means ± S.E. Calculations were done on at least 2250 configurations resulting from molecular dynamics simulations. The variation of free energy of binding, $\Delta G_{binding}$, was calculated with the linear interaction energy method (Equation 2) using $\alpha = 0.476$, $\beta = 0.165$, and $\gamma = 0$ (25). Calculations with other parameter sets are shown in the supplemental material. $\Delta\Delta G_{binding}$ is defined as $\Delta G_{binding} - \Delta G^{control}_{binding}$ where "control" is the wild type model with a bound ATP for AtClCa and hClC5, respectively.

Model	Ligand	ΔV^{vdW}_{l-s} l	ΔV^{elec}_{l-s}	$\Delta G_{binding}$	$\Delta G_{binding}$
		kcal/mol	*kcal/mol*	*kcal/mol*	*kcal/mol*
AtClCa	ATP	−21.0 ± 0.4	−73.8 ± 0.6	−22.2 ± 0.6	
	ADP	−10.1 ± 0.5	−21.5 ± 0.4	−8.4 ± 0.4	−13.8 ± 0.7
	AMP	−149.8 ± 0.4	−3.0 ± 0.3	−26.1 ± 0.3	3.9 ± 0.5
H620A	ATP	−18.7 ± 0.3	−45.2 ± 1.0	−16.4 ± 0.3	−5.8 ± 0.9
D753A	ATP	−17.6 ± 0.4	23.6 ± 1.0	−4.5 ± 0.2	−17.7 ± 0.6
hClC5	ATP	−14.4 ± 0.4	−17.6 ± 1.9	−9.8 ± 0.6	
	ADP	−16.0 ± 0.4	8.4 ± 1.2	−6.2 ± 0.5	−3.5 ± 0.8
	AMP	−23.7 ± 0.2	11.1 ± 0.8	−9.4 ± 0.3	−0.3 ± 0.6

the transmembrane electric field, presumably at the cytoplasmic water-membrane interface, where the C terminus region of the protein would be settled.

As these results indicate that the C terminus region of AtCLCa might be involved in the recognition and binding of ATP, we used the structure of the hCLC-5 C-terminal domain (15) as a template for modeling AtCLCa C terminus. Although the sequence homology of these two protein regions is not particularly high (19% identity and 45% similarity), they have a remarkable secondary structure superposition and the same organization of CBS domains. Indeed, the homology model obtained for AtCLCa conforms to all common structural criteria, including a Ramachandran plot comparable with the template (data not shown). In the AtCLCa model we could accommodate the ATP molecule in the same position as in the hCLC5 template, *i.e.* bound to the interface of the CBS domains, with the adenine moiety deeply inserted into the protein.

ATP is contacted by residues conserved in hCLC-5 and AtCLCa such as Asp-727/753 and non-conserved residues such as Tyr-617/His-620. Consequently, we attempted to perturb the putative binding site of ATP by introducing in positions 620 and 753 of AtCLCa, as suggested by our molecular model. The experimental results obtained upon expression of the mutated proteins in the null mutant background revealed that the effect of ATP was abolished by the D753A mutation, whereas it was unaffected by the H620A mutation.

In an attempt to validate our model of nucleotide binding to the C-terminal CBS motifs of AtCLCa, we estimated the free energy of binding for the wild type and the mutant models. We used a semi-empirical approach, linear interaction energy, that requires the parameterization of the proportionality factors, α, β, and γ, using known structural and functional data of similar proteins and ligands (24–26). As the only available set of data deals with the ATP, ADP, and AMP binding to hCLC-5, with a null variation on the binding constant, we decided to use the set of parameters reported in the literature that better represent the known data. These parameters result in a $\Delta G_{binding}$ as similar as possible to the experimental data, with a minimal variation for the $\Delta G_{binding}$ between the three ligands. We are aware that such assumption will result on a low quantitative significance results. Indeed, on the basis of the previous considerations on the relatively small changes of energy binding between ATP and ADP, the model seems to describe the energy variation with an uncertainty that is in the order of 4 kcal/mol, *i.e.* definitely larger of the data error reported in Table 1. Nevertheless, theoretical data are qualitatively consistent with experimental data, which indicate that the affinity of nucleotides for AtCLCa is ATP ≈ AMP > ADP. On the other hand, the effects of AtCLCa mutations are such that ATP affinity sequence is wild type > H620A > D753A. Therefore, the agreement between experimental data and model predictions validates our molecular model describing the binding of ATP to AtCLCa. Taken together, these evidences support the idea that ATP inhibits AtCLCa-mediated currents through interaction with its C-terminal CBS motifs. The conservation of CBS domain in eukaryotic CLC suggests that some mechanisms are conserved in nucleotide binding.

The finding that the D753A mutation abolishes ATP effects is in agreement with the results on the hCLC-5 mutant D727A (15). It is interesting to notice that CBS domains, which mediate nucleotide binding to other proteins such as the γ1 subunit of the AMPK kinase (17), present an aspartate in an equivalent position. Instead, CBS of CLC channels, which do not bind nucleotides (such as hCLCKa and CLC-0), do not harbor an aspartate in an equivalent position (14, 32). Conversely CLC-1, which has been suggested to be also modulated by intracellular ATP (9–11), has a glutamate in the equivalent position. We could speculate that this difference as well as the dependence of the ATP effect on the oxido-reduction of the protein suggested for ClC-1 (13) may depend on a different interaction between the nucleotides and the protein. The presence of an aspartate in the CBS domain (Fig. 4*b*) was consistently found to be associated with nucleotide binding to CBS segments.

The other nucleotides, ADP and AMP, displayed only minor effects on AtCLCa current. Competition experiments showed that AMP, but not ADP, competes with ATP at the AtCLCa binding site. Our results on AtCLCa differ from experiments reported for hCLC-5 (15), which binds equally well AMP, ADP, and ATP. This difference in nucleotide selection between AtCLCa and hCLC-5 presumably depends on the differences in the residues that contact the phosphate groups of the nucleotides (supplemental Fig. 2 and 3 (15)).

The addition of Mg-ATP to the bath solution in the absence of $BafA_1$ allowed visualizing the activity of the H^+-ATPase together with that of AtCLCa (Fig. 1). Despite the fact that the H^+-ATPase currents across the vacuolar membrane were measured before (28, 33), this is the first time that an intracellular CLC antiporter and a proton pump are shown working together in the same intracellular membrane. Therefore, both transport systems might be saturated at physiological ATP concentration (in the millimolar range). However, competition between AMP and ATP in AtCLCa suggests that the transport mediated by AtCLCa *in vivo* could be modulated by the ATP/AMP ratio. This regulation might be correlated with nitrate metabolism in plants. Nitrate storage in the vacuole takes place during the night, when nitrate reductase is inactive. NO_3^- is then released from the vacuole during the day, when the requirement of nitrate by nitrate reductase is high (34). The cytosolic ATP and AMP pools have been shown to regulate nitrate reductase activity and to vary together with the photosynthetic status of the cell (35). Therefore, the competition between ATP and AMP at the AtCLCa binding site could be a physiologically relevant process; an increase of the AMP/ATP ratio could remove the inhibition of AtCLCa and consequently increase the nitrate flow into the vacuole when the photosynthetic activity decreases. However, even under physiological cytosolic nitrate concentrations we do not observe a complete inhibition of AtCLCa-mediated nitrate influx by ATP but, rather, a decrease in the in the order of 50% (Fig. 3). This indicates that there is either always a basal activity of AtCLCa present or that other mechanisms may be required for its regulation in addition to nucleotide binding.

Acknowledgment—We thank Dr. R. Noto for invaluable assistance on setting-up the computer facilities.

REFERENCES

1. Forde, B. G. (2000) *Biochim. Biophys. Acta* **1465,** 219–235
2. Martinoia, E., Heck, U., and Wiemken, A. (1981) *Nature* **289,** 292–294
3. De Angeli, A., Monachello, D., Ephritikhine, G., Frachisse, J. M., Thomine, S., Gambale, F., and Barbier-Brygoo, H. (2006) *Nature* **442,** 939–942
4. Geelen, D., Lurin, C., Bouchez, D., Frachisse, J. M., Lelièvre, F., Courtial, B., Barbier-Brygoo, H., and Maurel, C. (2000) *Plant J.* **21,** 259–267
5. Accardi, A., and Miller, C. (2004) *Nature* **427,** 803–807
6. Picollo, A., and Pusch, M. (2005) *Nature* **436,** 420–423
7. Scheel, O., Zdebik, A. A., Lourdel, S., and Jentsch, T. J. (2005) *Nature* **436,** 424–427
8. Accardi, A. (2008) *J. Gen. Physiol* **131,** 105–108
9. Bennetts, B., Parker, M. W., and Cromer, B. A. (2007) *J. Biol. Chem.* **282,** 32780–32791
10. Bennetts, B., Rychkov, G. Y., Ng, H. L., Morton, C. J., Stapleton, D., Parker, M. W., and Cromer, B. A. (2005) *J. Biol. Chem.* **280,** 32452–32458
11. Tseng, P. Y., Bennetts, B., and Chen, T. Y. (2007) *J. Gen. Physiol.* **130,** 217–221
12. Zifarelli, G., and Pusch, M. (2008) *J. Gen. Physiol.* **131,** 109–116
13. Zhang, X. D., Tseng, P. Y., and Chen, T. Y. (2008) *J. Gen. Physiol.* **132,** 421–428
14. Meyer, S., and Dutzler, R. (2006) *Structure* **14,** 299–307
15. Meyer, S., Savaresi, S., Forster, I. C., and Dutzler, R. (2007) *Nat. Struct. Mol. Biol.* **14,** 60–67
16. Bateman, A. (1997) *Trends Biochem. Sci.* **22,** 12–13
17. Townley, R., and Shapiro, L. (2007) *Science* **315,** 1726–1729
18. Hosy, E., Duby, G., Véry, A. A., Costa, A., Sentenac, H., and Thibaud, J. B. (2005) *Plant Methods* **1,** 14
19. De Angeli, A., Monachello, D., Ephritikhine, G., Frachisse, J. M., Thomine, S., Gambale, F., and Barbier-Brygoo, H. (2009) *Philos. Trans. R. Soc. Lond. B. Biol. Sci.* **364,** 195–201
20. Neher, E. (1992) *Methods Enzymol.* **207,** 123–131
21. Arnold, K., Bordoli, L., Kopp, J., and Schwede, T. (2006) *Bioinformatics* **22,** 195–201
22. Guex, N., and Peitsch, M. C. (1997) *Electrophoresis* **18,** 2714–2723
23. Phillips, J. C., Braun, R., Wang, W., Gumbart, J., Tajkhorshid, E., Villa, E., Chipot, C., Skeel, R. D., Kalé, L., and Schulten, K. (2005) *J. Comput. Chem.* **26,** 1781–1802
24. Aqvist, J., Medina, C., and Samuelsson, J. E. (1994) *Protein Eng.* **7,** 385–391
25. Hansson, T., Marelius, J., and Aqvist, J. (1998) *J. Comput. Aided Mol. Des.* **12,** 27–35
26. Jones-Hertzog, D. K., and Jorgensen, W. L. (1997) *J. Med. Chem.* **40,** 1539–1549
27. Wang, W., Wang, J., and Kollman, P. A. (1999) *Proteins* **34,** 395–402
28. Hedrich, R., Kurkdjian, A., Guern, J., and Flügge, U. I. (1989) *EMBO J.* **8,** 2835–2841
29. Bowman, E. J., Siebers, A., and Altendorf, K. (1988) *Proc. Natl. Acad. Sci. U.S.A.* **85,** 7972–7976
30. Laskowski, R. A., MacArthur, M. W., Moss, D. S., and Thornton, J. M. (1993) *J. Appl. Crystallogr.* **26,** 283–291
31. Hooft, R. W., Vriend, G., Sander, C., and Abola, E. E. (1996) *Nature* **381,** 272
32. Markovic, S., and Dutzler, R. (2007) *Structure* **15,** 715–725
33. Gambale, F., Kolb, H., Cantu, A. M., and Hedrich, R. (1994) *Eur. Biophys. J.* **22,** 399–403
34. Cookson, S. J., Williams, L. E., and Miller, A. J. (2005) *Plant Physiol.* **138,** 1097–1105
35. Kaiser, W. M., and Spill, D. (1991) *Plant Physiol.* **96,** 368–375